Electronic Supplementary Material (ESI) for Physical Chemistry Chemical Physics.

Supporting Information

Two-dimensional $Mo_{1-x}B_2$ with ordered metal vacancies obtained for advanced thermoelectric applications based on first-principles calculations

Jie Pu[1], Ziyu Hu[1,*], Xiaohong Shao[1,*]

[1]*College of Mathematics and Physics, Beijing University of Chemical Technology, Beijing, 100029, China*

**Correspondence and requests for materials should be addressed to X. H. Shao (shaoxh@mail.buct.edu.cn) and Z. Y. Hu (huziyu@mail.buct.edu.cn)*

Table S1. Lattice Constants and bonds length of $Mo_{1-x}B_2$ (x=0, 0.05, 0.10, 0.125, 0.15).

	a=b(Å)	c(Å)	B-B	Mo-Mo	Mo-B
MoB_2	10.271	23.720	1.708	2.986	2.221
$Mo_{0.95}B_2$	10.271	23.720	1.712	2.890	2.264
$Mo_{0.9}B_2$	10.271	23.720	1.701	2.830	2.178
$Mo_{0.875}B_2$	10.271	23.720	1.717	2.786	2.222
$Mo_{0.85}B_2$	10.271	23.720	1.728	2.774	2.123

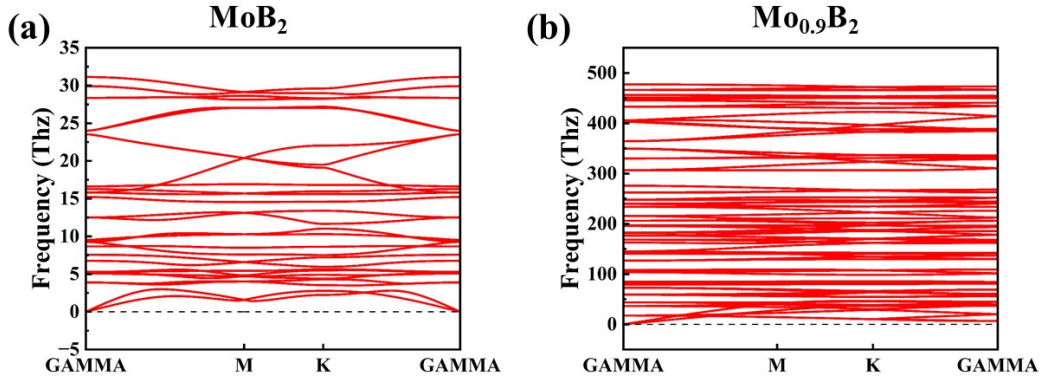

Figure S1. Phonon spectra of MoB_2 (a) and $Mo_{0.9}B_2$ (b)**.**

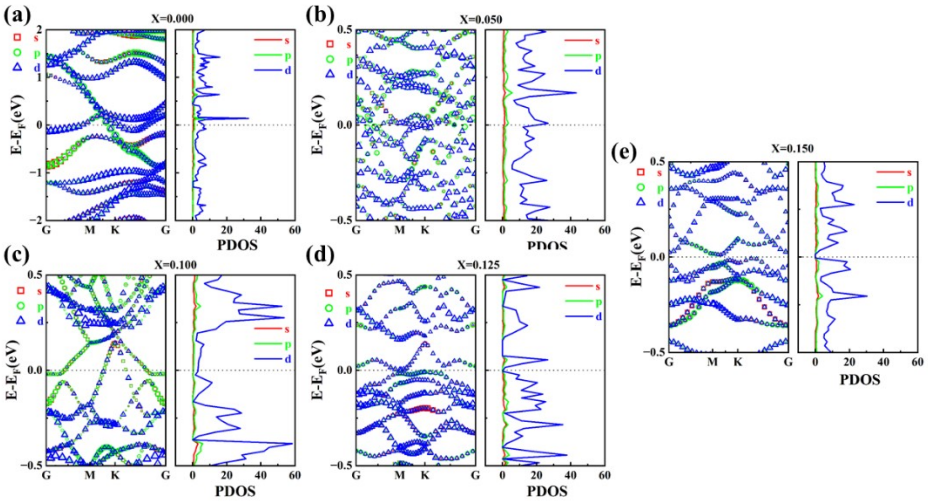

Figure S2. The orbital projection energy bands and the density of projected states of Mo in $Mo_{1-x}B_2$, with (a) x = 0.000, (b) x = 0.050, (c) x = 0.100, (d) x = 0.125, (e) x = 0.150 calculated by PBE.

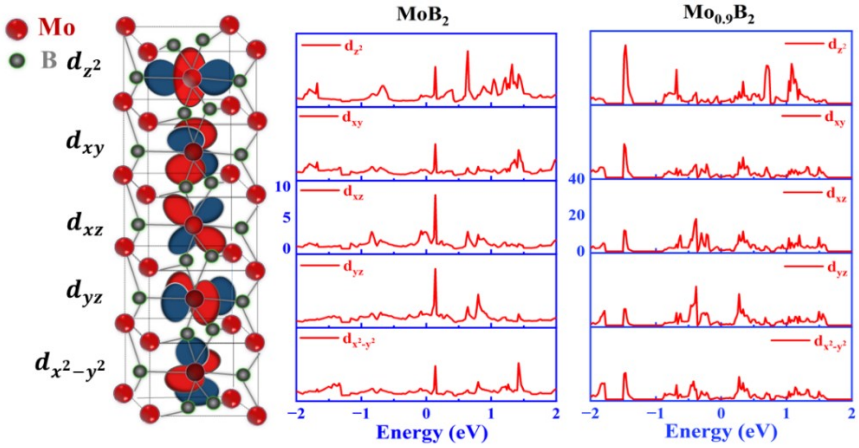

Figure S3. Bonding analysis of Mo atoms. Partial orbitals diagram comparisons between MoB_2 and $Mo_{0.9}B_2$.

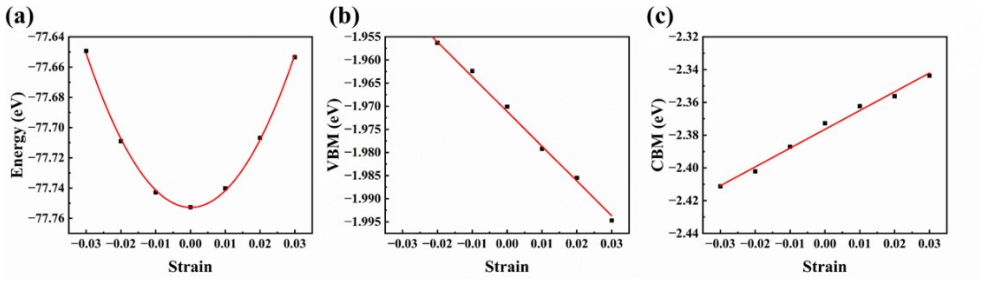

Figure S4. (a) The total energy of MoB_2 is fitted along the a-axis direction, (b) the energy changes of electrons at valence band maximum (VBM), (c) the energy changes of holes at the conduction band minimum (CBM).

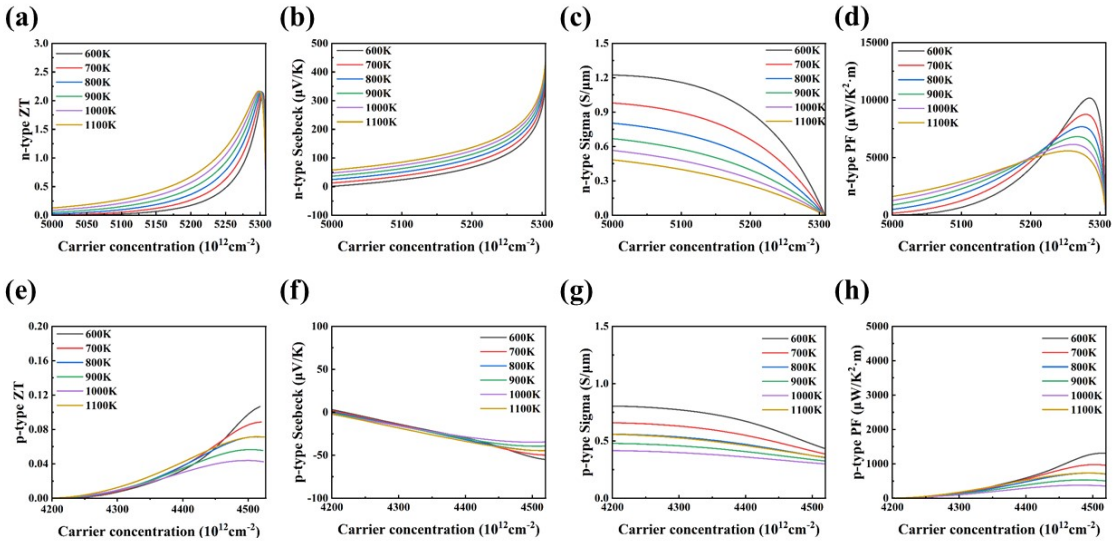

Figure S5. Thermoelectric parameters of *n*-type and *p*-type monolayer MoB_2 varied with carrier concentration. (a) *n*-type ZT value, (b) *n*-type Seebeck coefficient, (c) *n*-type conductivity, (d) *n*-type power factor, (e) *p*-type ZT value, (f) *p*-type Seebeck coefficient, (g) *p*-type conductivity, (h) *p*-type power factor.

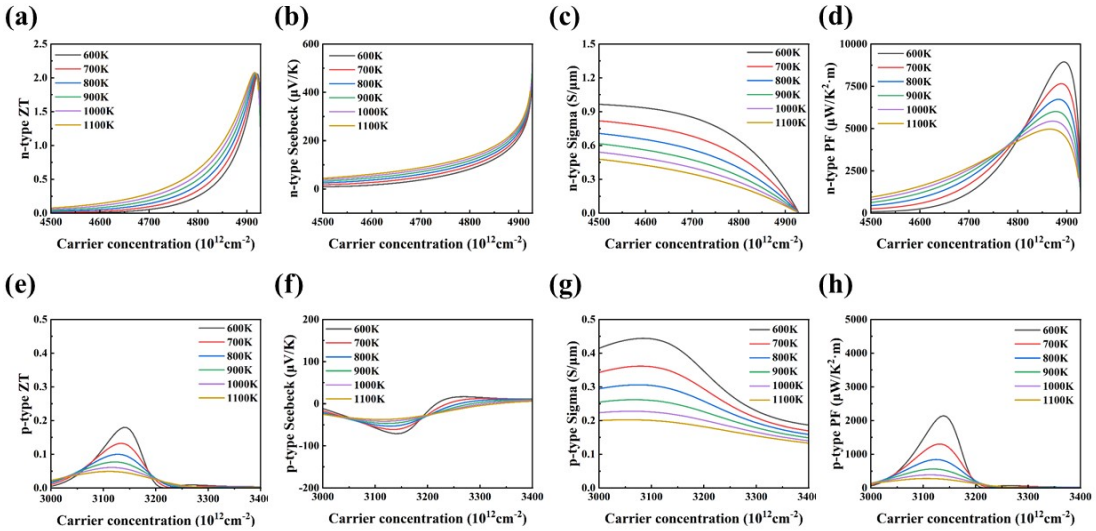

Figure S6. Thermoelectric parameters of *n*-type and *p*-type monolayer $Mo_{0.95}B_2$ varied with carrier concentration. (a) *n*-type ZT value, (b) *n*-type Seebeck coefficient, (c) *n*-type conductivity, (d) *n*-type power factor, (e) *p*-type ZT value, (f) *p*-type Seebeck coefficient, (g) *p*-type conductivity, (h) *p*-type power factor.

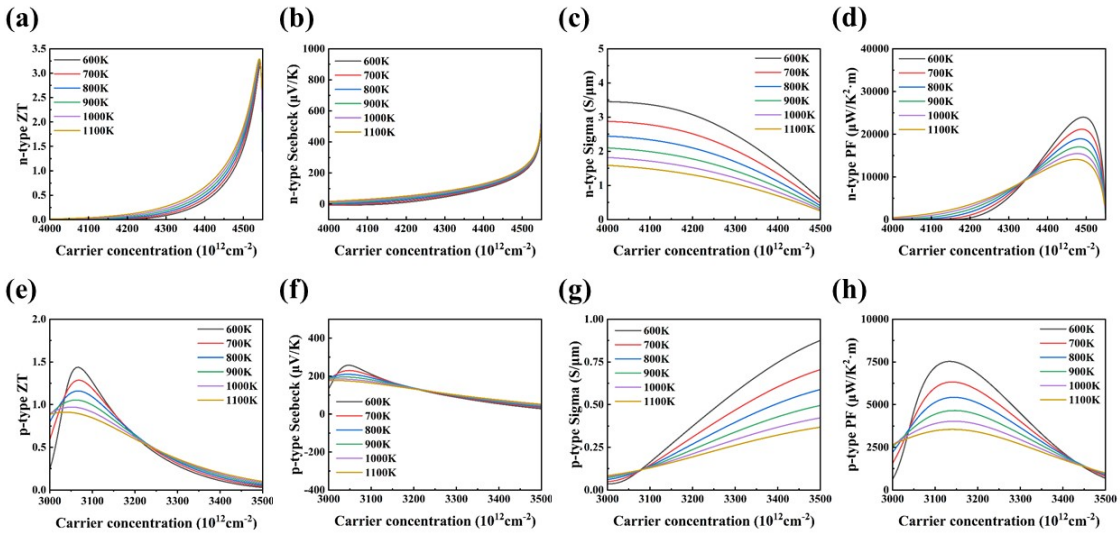

Figure S7. Thermoelectric parameters of *n*-type and *p*-type monolayer $Mo_{0.9}B_2$ varied with carrier concentration. (a) *n*-type ZT value, (b) *n*-type Seebeck coefficient, (c) *n*-type conductivity, (d) *n*-type power factor, (e) *p*-type ZT value, (f) *p*-type Seebeck coefficient, (g) *p*-type conductivity, (h) *p*-type power factor.

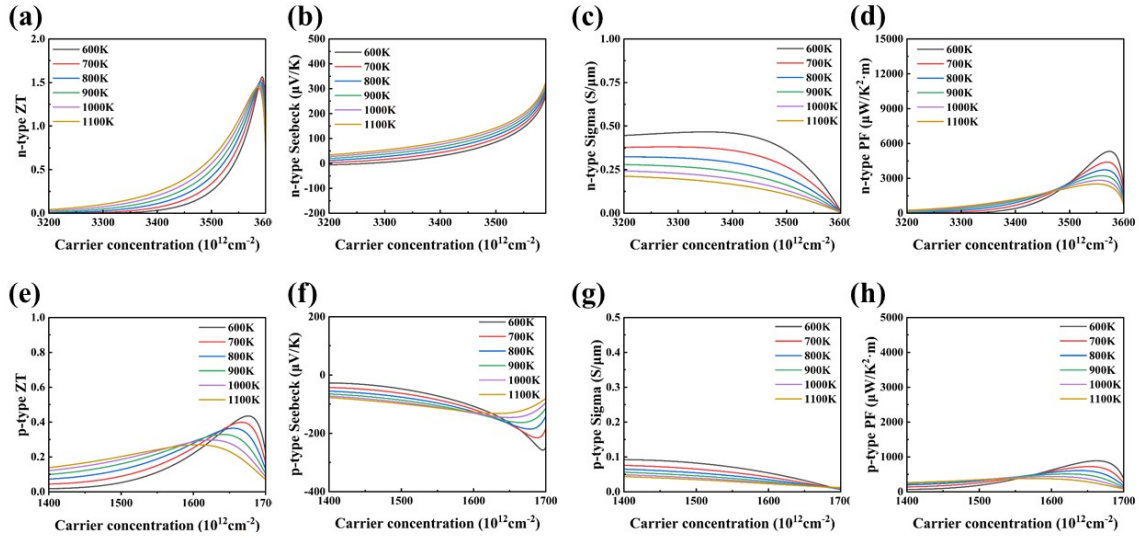

Figure S8. Thermoelectric parameters of *n*-type and *p*-type monolayer $Mo_{0.875}B_2$ varied with carrier concentration. (a) *n*-type ZT value, (b) *n*-type Seebeck coefficient, (c) *n*-type conductivity, (d) *n*-type power factor, (e) *p*-type ZT value, (f) *p*-type Seebeck coefficient, (g) *p*-type conductivity, (h) *p*-type power factor.

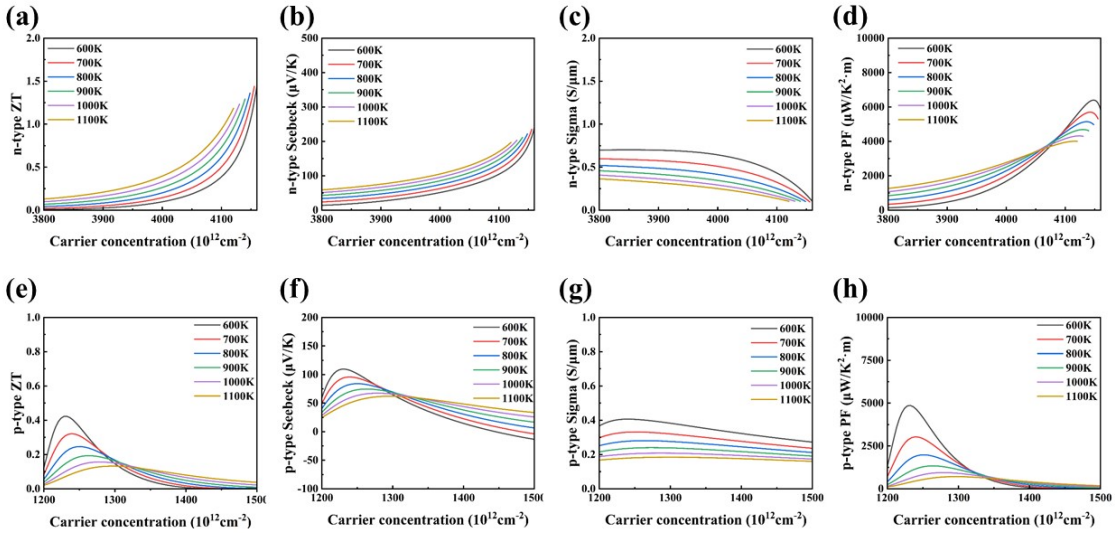

Figure S9. Thermoelectric parameters of *n*-type and *p*-type monolayer $Mo_{0.85}B_2$ varied with carrier concentration. (a) *n*-type ZT value, (b) *n*-type Seebeck coefficient, (c) *n*-type conductivity, (d) *n*-type power factor, (e) *p*-type ZT value, (f) *p*-type Seebeck coefficient, (g) *p*-type conductivity, (h) *p*-type power factor.